Proceedings of the Combustion Institute 41 (2025) 105788

Contents lists available at ScienceDirect

Proceedings of the Combustion Institute

journal homepage: www.elsevier.com/locate/proci

Kinetic study of ozone-sensitized low- and high-temperature oxidation of dimethyl carbonate

Bowen Liu, Rui Bo, Hao Zhao *

School of Mechanics and Engineering Science, Peking University, Beijing 100871, China

ARTICLE INFO

Keywords:
Lithium-ion batteries
Dimethyl carbonate
Low temperature chemistry
Temperature-independent coefficient
Ozone

ABSTRACT

The low- and high-temperature oxidation of dimethyl carbonate (DMC), a key electrolyte component in lithium-ion batteries (LIBs), was carried out with ozone (O_3) addition by using an atmospheric pressure Jet Stirred Reactor (JSR) from 400 to 1200 K. Kinetic analysis of DMC oxidation was conducted using the coupled Plug Flow Reactor-Perfectly Stirred Reactor (PFR-PSR) module. Without O_3 addition, the oxidation of DMC initiated at 950 K with no low-temperature reactivity. However, the low-temperature chemistry of DMC was observed from 450 K with O_3 addition, and O_3 significantly enhanced the low-temperature reactivity of DMC. Two kinetic models with incorporating the O_3 sub-model were employed and predicted the experimental data reasonably well, even though slightly overpredicted DMC oxidation above 550 K under the fuel-lean condition. Furthermore, a temperature-independent coefficient (TIC) behavior of DMC with O_3 addition was observed between 600 and 950 K both in experiments and simulations, which was associated with the pyrolysis of DMC radicals to CH_2O and CO_2, and then to CO, while the low-temperature oxidation pathway through 1st and 2nd O_2 addition and CO oxidation to CO_2 was negligible. The fast pyrolysis reaction rates of O_3 and DMC radicals, such as $CH_3OC(=O)OCH_2$ and $CH_3OC(=O)$, explain the TIC behavior in the pathway and sensitivity analyses. This work used O_3 to mimic the oxidizing environment in LIBs by providing active atomic oxygen, and implied that the early degradation of LIBs could be attributed to the low-temperature oxidation of DMC with reactive oxygen species. It provides kinetic evidence for a higher level of CO_2 and a lower level of CO in the initial stage of the thermal runaway in LIBs.

1. Introduction

Lithium-ion batteries (LIBs) are widely applied in electronic devices and new energy vehicles for their light weight and high energy density [1]. Abusive operating conditions, including mechanical (deformation/penetration), thermal (external heating), and electrical (short circuit/overcharge) [2–5], can trigger thermal runaway in LIBs, which is a significant safety concern for LIBs applications. Additionally, the flammability and decomposition of the electrolyte are closely related to the early initiation of thermal runaway [4], and a thorough understanding of the oxidative behavior of the electrolyte components, especially at low temperature, is crucial for improving the thermal safety of LIBs.

Dimethyl carbonate (DMC) is a major component in electrolytes of LIBs, enabling lithium salt ion transport between the cathode and anode [6]. Previous studies have carried out extensive work on the fundamental combustion characteristics of DMC, such as ignition delay time [7,8], laminar flame speed [6], and high-temperature oxidation [9,10]. However, most of the previous studies focused on DMC as a diesel additive [6–14] rather than an electrolyte component. Therefore, further studies are needed on DMC as an electrolyte component. Recent studies indicate that reactive oxygen species (e.g., singlet oxygen $^1O_2$ or atomic oxygen O) are associated with early oxidation of electrolytes [15,16]. Wandt et al. [16] first discovered the release of excited singlet oxygen ($^1O_2$) in LIBs, and proposed the assumption that the oxidation of the electrolyte was probably related to the $^1O_2$. Jung et al. [17] inferred that the early CO_2 originated from some kind of reactive oxygen (reactive O or $^1O_2$) released from the positive electrode reacting rapidly with the electrolyte instead of electro-chemical oxidation. Rinkel et al. [15] investigated the decomposition and gas generation mechanisms of NMC ($LiNi_xMn_yCo_{1-x-y}O_2$) and LCO ($LiCoO_2$) cathode surfaces using in situ gas measurements and NMR techniques. It was found that $^1O_2$ was released from the transition metal oxides to participate in the oxidation of the electrolyte at high potentials, producing CO_2, CO, and H_2O. Further, common electrolyte components including dimethyl carbonate (DMC),

* Corresponding author.
E-mail address: h.zhao@pku.edu.cn (H. Zhao).

https://doi.org/10.1016/j.proci.2025.105788
Received 28 May 2025; Accepted 22 July 2025
Available online 6 August 2025

diethyl carbonate (DEC), and ethylene carbonate (EC) do not react directly with oxygen in the gas phase at temperature below 650 K [18]. Nevertheless, thermal runaway in LIBs typically occurs between 400 and 500 K [19], which further supports the possibility that strong oxidizers foster the oxidation of the electrolyte, accelerating thermal runaway at low temperature. However, the interaction mechanisms between electrolyte components and reactive oxygen remain unclear, and the effect of reactive oxygen on the thermal runaway of LIBs is still not well comprehended.

Ozone (O_3), as a strong oxidizer, can decompose rapidly to generate reactive O and oxygen O_2 (including $^1O_2$ [20]) at the temperature above 400 K [21]. This study aims to use O_3 to mimic the oxidizing environment in LIBs by providing active atomic oxygen, sensitizing the low-temperature oxidation of DMC, and enhancing the understanding of the thermal runaway in LIBs involved in the electrolyte oxidation at low temperature. In previous work, we explored the effect of O_3 on DEC oxidation using a laminar flow reactor [18]. However, DMC, as a more widely used electrolyte solvent representative, differs from DEC in thermophysical properties and reactivity. In this work, we investigate the ozone-sensitized low- and high-temperature oxidation mechanisms of DMC through experiments and kinetic simulations.

2. Methods

2.1. Experimental setups

The experiments were performed in an atmospheric pressure jet stirred reactor (JSR). The schematic of JSR configuration is shown in Fig. 1. The JSR with an internal volume of 30.5 cm^3 was made of fused quartz to avoid wall reactions. In analogy to the JSR design of Dagaut et al. in [22], it had four nozzles of 1 mm inner diameter in the center of JSR to generate intense turbulence and homogeneous mixing. A secondary nitrogen stream carried vaporized DMC gas from the evaporator tank, and then mixed with oxidizer stream (O_2/O_3) before entering the JSR. Finally, the mixed gas and mainstream nitrogen were merged at the JSR inlet. To avoid over-preheating, the mixed gas was introduced into the reactor through an aperture in the side wall of the heating oven. As a result, the tube, which was 5.5 cm in length and 2 mm inner diameter (approximately 0.17 cm^3, 0.57 % of the JSR internal volume), was located inside the heating oven. Nevertheless, the preheating was found to be non-negligible in the present study. The volumetric flow rates were regulated by mass flow controllers (MKS, 0.5 % uncertainty), which were calibrated by a gas calibrator (Drycal 530+, accuracy ±1 %). The purity of the gases was greater than 99.999 %. Liquid fuel was infused into the preheated evaporator through a high-precision and high-pressure liquid syringe pump (CHEMYX FUSION 6000-X). Meanwhile, the temperature at the inlet, center, and outlet of JSR were measured by inserting a K-type thermocouple from the exit, and the accuracy of temperature control within the JSR was within ±2.5 K. A sonic probe with an inner diameter of 100 μm was located at the outlet of JSR, simultaneously, a vacuum chamber was utilized for sampling with the purpose of reducing the influence of sampling on the internal flow in the JSR, as well as decreasing the residence time of the reaction gas in the sampling tube. A gas chromatography (GC, Agilent 8890) equipped with two Flame Ionization Detectors (FID) and a Thermal Conductivity Detector (TCD) was used to analyze the product concentration. The species measurements were repeated two times under every experimental condition with a repeatability uncertainty less than 5 %.

An ozone generator was employed to generate O_3 at room temperature using dielectric barrier discharge (DBD). In this work, O_3 was generated by discharging in a pure oxygen stream, instead of air, to avoids the nitrogen-related reactions. O_3 can be absorbed in the UV-NIR band (200 ~ 1100 nm) [23] making it well-suited for quantification by the absorption spectroscopy technique. The O_3 mole fraction was measured using UV light at 253.7 nm, where O_3 is strongly absorbed, as is shown in Fig. 2. The UV light at 253.7 nm was emitted by a mercury lamp (BHK Analamp), and then passed through a quartz UV absorption cell of 10 cm in length. The absorbed light was received by a photodiode with a filter, and the O_3 mole fraction was obtained by amplifying and processing the voltage signal.

A brief description of the O_3 mole fraction calculations is as follows. Under the condition that the absorption cross-section coefficient (σ) and the optical range (L) are known, the O_3 mole fraction can be inverted according to the Beer-Lambert Law by monitoring the intensity of the initial and absorbed light:

$$I_{out} = I_{in}\exp(-\alpha_0 \cdot C \cdot L) \tag{1}$$

where I_{out}, I_{in}, α_0, C, and L are the outgoing light intensity, the incident light intensity, the absorption coefficient, the mole fraction of absorbing medium, and the optical range, respectively. Then, Eq. (1) can be combined with the ideal gas equation of state:

$$-\ln\left(\frac{I_{out}}{I_{in}}\right) = \alpha_0 \cdot C \cdot L = C \cdot N_0 \cdot \sigma \cdot L = C \cdot \frac{PN_A}{RT} \cdot \sigma \cdot L \tag{2}$$

where C is the gas volume concentration to be measured in ppm; N_0 is the number of molecules per unit volume in molecules/cm^3; σ is the absorption cross-section of the component to be measured in cm^2/molecules; L is the optical range in cm; P is the pressure in Pa; T is the temperature in K; N_A is Avogadro constant; R is the gas constant.

2.2. Kinetic simulations

In this work, Chemkin-pro [24] was employed for the kinetic simulations. We found that a single Perfectly Stirred Reactor (PSR) module was not able to predict the experimental results well, even after replacing multiple mechanism models. Although the size of fuel/oxidizer tube in the heating oven was quite small (0.57 % of the JSR internal volume), it needed to be considered for a more accurate prediction of the experimental trend. Therefore, we added two Plug Flow Reactor (PFR) modules coupled with the PSR module to simulate the preheating section. In detail, the fuel injection line was modeled using a PFR module,

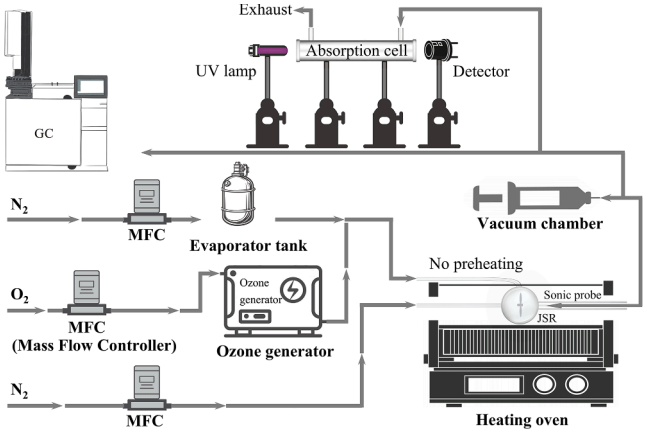

Fig. 1. Experimental setups.

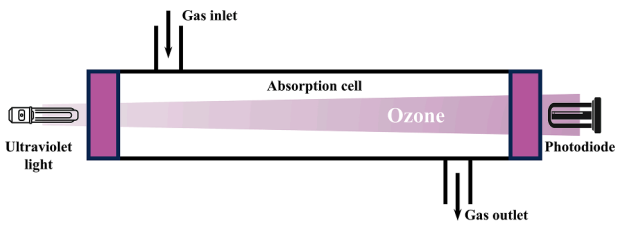

Fig. 2. Measurement of ozone concentration.

featuring an inner diameter of 2 mm and length of 55 mm, specifically designed to deliver DMC, O_2, N_2 (600 ml/min), and O_3 mixtures. The remaining N_2 was modeled using another PSR module with an inner diameter of 20 mm and length of 120 mm. The detailed DMC mechanisms proposed by Sun et al. [9] and Alzueta et al. [7] were coupled with Princeton O_3 sub-mechanism [18], in which the O_3 decomposition reaction and reactions with O, H, OH, HO_2, H_2O, CO, HCO, and CH_3 were considered.

2.3. Experimental conditions

The experimental conditions in this study are listed in Table 1. The inlet volumetric flow rate is fixed at 2500 ml/min at 298 K, while the residence time (τ) can be calculated by:

$$\tau = \frac{V_0}{u}\cdot\frac{T_0}{T} \tag{3}$$

where V_0, u, T_0, and T represent the internal volume of JSR, the total volumetric flow rate of the JSR inlet at room temperature, room temperature at 298 K, and the temperature in JSR, respectively.

3. Results and discussion

3.1. The mole fraction of main species

Mole fractions of the main species with temperature in the oxidation of DMC with and without O_3 addition at $\phi = 0.5$ are depicted in Fig. 3, including DMC, O_2, O_3, CO_2, CO, and C_2H_4. For DMC, we differentiate the low- and high-temperature oxidation regions in green between 450 and 950 K and in orange between 950 and 1150 K, respectively. Without O_3 addition, DMC is almost not consumed below 950 K, while its low-temperature oxidation starts from 450 K with O_3 addition, where O_3 decomposes at this temperature in Fig. 3(c), simultaneously. The observation above corresponds to our previous findings in [18,25]. Therefore, it shows that a low-temperature oxidation of DMC has been observed in experiments with O_3 by reducing the onset temperature of oxidation from 950 to 450 K. It is noted that a temperature-independent coefficient (TIC) behavior of DMC oxidation with O_3 addition is first observed in a broad low temperature range of 600 - 900 K in Fig. 3(a), where the fuel concentration has a weak temperature dependence in this "frozen" region. The similar behaviors in the mole fraction curves of O_2, CO_2, and CO in Fig. 3(b), 3(d), and 3(e), confirmed the TIC phenomenon of DMC with O_3 addition. When the temperature is above 900 K, the high temperature oxidation of DMC with O_3 addition starts and produces major intermediates and products promptly. As to the model simulation, it captures the DMC oxidation without O_3 addition well, while slightly overpredicts the consumption of DMC in the TIC region in Fig. 3(a). It implies that uncertainty may exist in the coupling reactions between DMC and O_3, and the fuel consumption pathways in the TIC region.

The mole fraction of CH_4, C_2H_6, C_2H_2, and dimethyl ether (DME) are depicted in Fig. S1. Both models generally overestimate the formation of these species in the TIC region, especially for C_2H_6 and CH_4, and possess high uncertainties in predicting the DME profile. Furthermore, the regeneration of small hydrocarbons, such as CH_4, C_2H_6, and C_2H_4, is observed above 1100 K, which may be related to the rapid pyrolysis of DMC in this temperature range, while this phenomenon has not been captured in the present models.

As to the fuel-rich condition ($\phi = 2.0$), the temperature evolutions of major intermediates and products are plotted in Fig. 4 and Fig. S2. Even though the O_3 mole fraction in the fuel-rich case is only 203 ppm, similar promoting effect of O_3 addition on DMC oxidation and TIC behavior have been observed in Fig. 4(a).

3.2. Reaction flux analysis

To explain the TIC behavior in the oxidation of DMC in experiments, we perform the pathway analysis of DMC with 911 ppm O_3 addition at low (550 K) and high (1050 K) temperature, respectively, at $\phi = 0.5$ in Fig. 5. There are three main pathways for the consumption of DMC, including two pyrolysis channels and one oxidation channel. At a low temperature of 550 K, the consumption of DMC mainly follows the oxidation pathway with O and OH, which are mainly produced from O_3 decomposition [18,25]. Then, the DMC radical, $CH_3OC(=O)OCH_2$, produces CH_2O, CO_2, and CH_3 through two pyrolysis steps, which exhibit weak temperature dependence due to their fast reaction rates. On the other hand, it is known from our previous study that O_3 decomposition is the dominant and most sensitive reaction for the low-temperature oxidation of fuel in [18,25], which will also been shown in the sensitivity analysis later. O_3 is almost fully decomposed at 550 K in Fig 3(c), therefore, this reaction is also temperature-independent above 550 K. These two aspects above explain the TIC behavior of DMC in Fig. 3(a). Moreover, it is noted in Fig. 5 that the early formation of CO_2 from the pyrolysis of DMC radicals, such as $CH_3OC(=O)OCH_2$ and $CH_3OC(=O)$, instead of from CO in the typical pathways, and CO is mainly produced from CH_2O at 550 K. This finding is very crucial and provides kinetic support for higher level of CO_2 and lower level of CO in the initial stage of the thermal runaway in LIBs [26]. At high temperature of 1050 K, the pyrolysis channels of DMC appear. The formations of CH_3, CO, CO_2, C_2H_6, etc. follow the typical high temperature pathways.

The reaction pathways of DMC under the fuel-rich condition at $\phi = 2.0$, are depicted in Fig. 6. Compared to fuel-rich pathway, the pyrolysis channels become more important due to the low concentrations of O_2 and O_3.

3.3. Sensitivity analysis

The sensitivity analyses of DMC with and without O_3 addition are conducted by using Sun's model at $\phi = 0.5$, at 550 and 1050 K in Fig. 7 (a) and (b), respectively. The sensitivity analyses under fuel-rich condition at $\phi = 0.5$ with and without O_3 addition are depicted in Fig. S3 of the supplementary material.

The sensitivity coefficient S_i for DMC is defined as:

$$S_i = \frac{(\Delta X_{DMC}/X_{DMC})}{\Delta k_i/k_i} \tag{4}$$

where X_{DMC} is the mole concentration of DMC and k_i is the rate constant of i^{th} reaction.

At 550 K with O_3 addition in Fig. 7(a), the most sensitive reaction for DMC consumption is $O_3 + (M) = O_2 + O + M$, where O is formed and then oxidizes DMC to its radicals promptly. It corresponds to the low

Table 1
Experimental conditions.

Case	Residence time (s)	Fuels	Equivalent ratio, ϕ	Percentage of components (%)				Temperature range (K)	Flow rate (ml/min)
				DMC	O_2	O_3	N_2		
1	0.55 - 0.18	DMC	0.5	0.3000	1.8000	0	97.9000	400 - 1200	2500
2			2.0	0.3000	0.4500	0	99.2500		
3			0.5	0.3000	1.6634	0.0911	97.9455		
4			2.0	0.3000	0.4196	0.0203	99.2601		

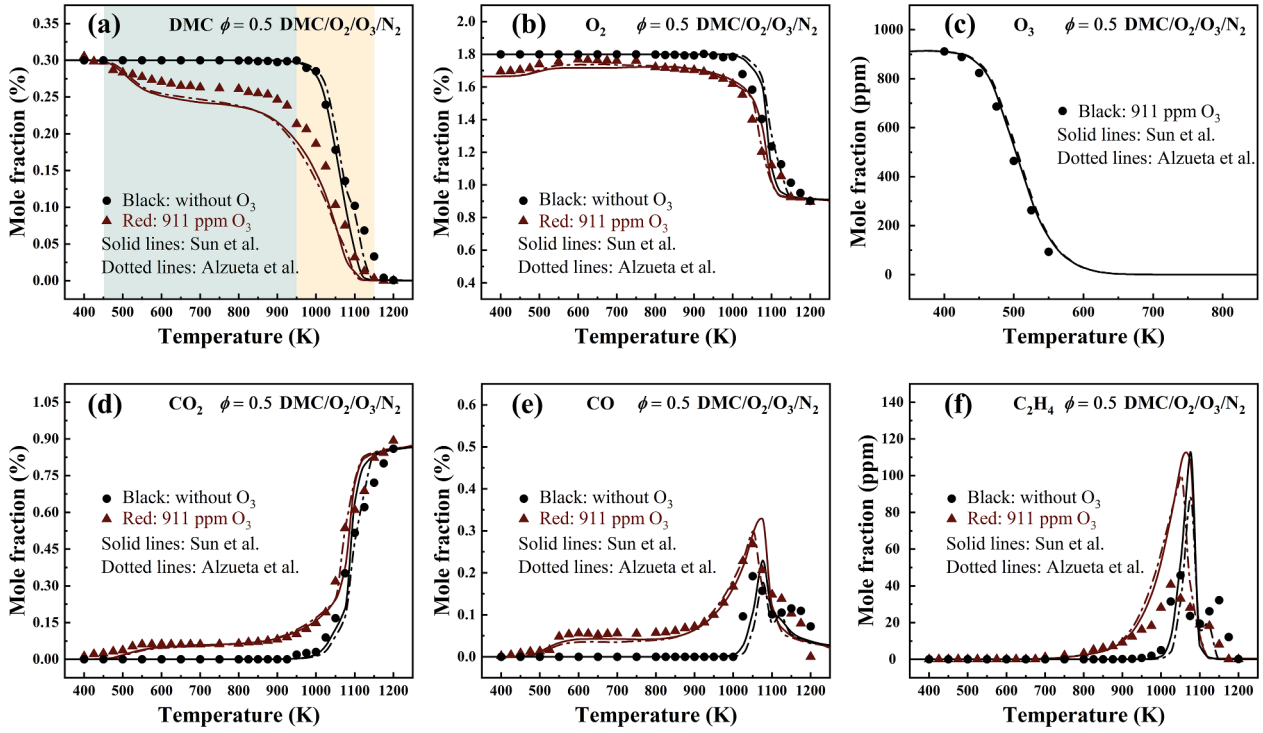

Fig. 3. Mole fractions of main species as a function of temperature at $\phi = 0.5$ with and without O_3 addition. The symbols represent the experimental data and the curves represent predictions of models, where the solid and dotted lines represent the predictions of Sun's model and Alzueta's model, respectively. (a) DMC; (b) O_2; (c) O_3; (d) CO_2; (e) CO; (f) C_2H_4.

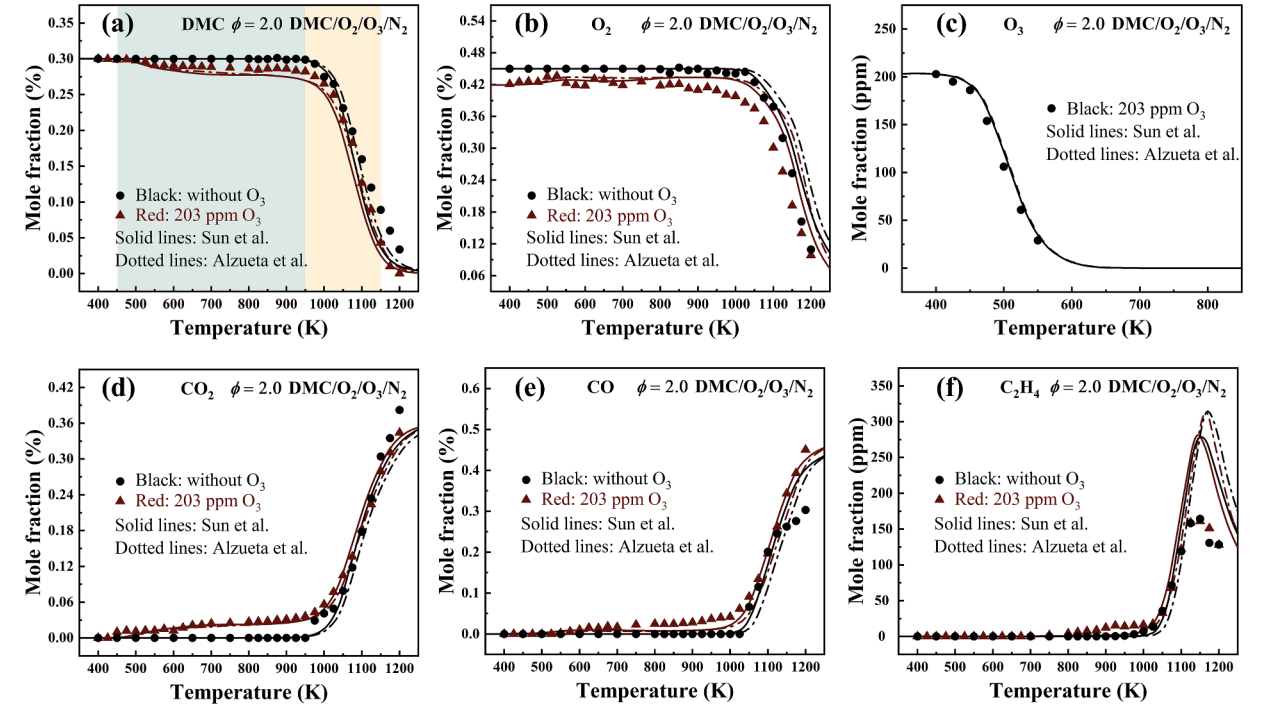

Fig. 4. Mole fractions of main species as a function of temperature at $\phi = 2.0$ with and without O_3 addition. The symbols represent the experimental data and the curves represent predictions of models, where the solid and dotted lines represent the predictions of Sun's model and Alzueta's model, respectively. (a) DMC; (b) O_2; (c) O_3; (d) CO_2; (e) CO; (f) C_2H_4.

temperature oxidation of DMC. The H-abstraction reaction of DMC with O and OH are, as expected, very sensitive. The reactions of $CH_3O_2 + O$ and $CH_2O + OH$ from small molecular chemistry are competing with the H-abstraction reaction of DMC. It has to be highly noted that the pyrolysis reactions of DMC radicals, such as $CH_3OC(=O)OCH_2$ and $CH_3OC(=O)$, are not sensitive here. That is because these pyrolysis reactions are very fast to form CO_2 and CH_3 with nearly 100 % conversions in the pathway analysis in Fig. 5. As such, perturbations in their

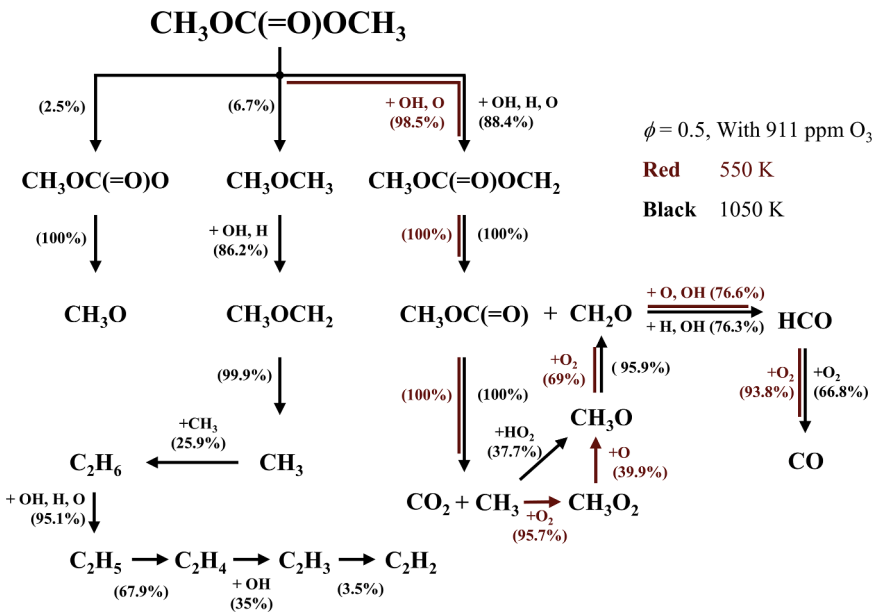

Fig. 5. The main consumption channels of DMC under low and high temperature at $\phi = 0.5$ with 911 ppm O_3 addition using Sun's model. Red and black represent the percentage at 550 K and 1050 K, respectively.

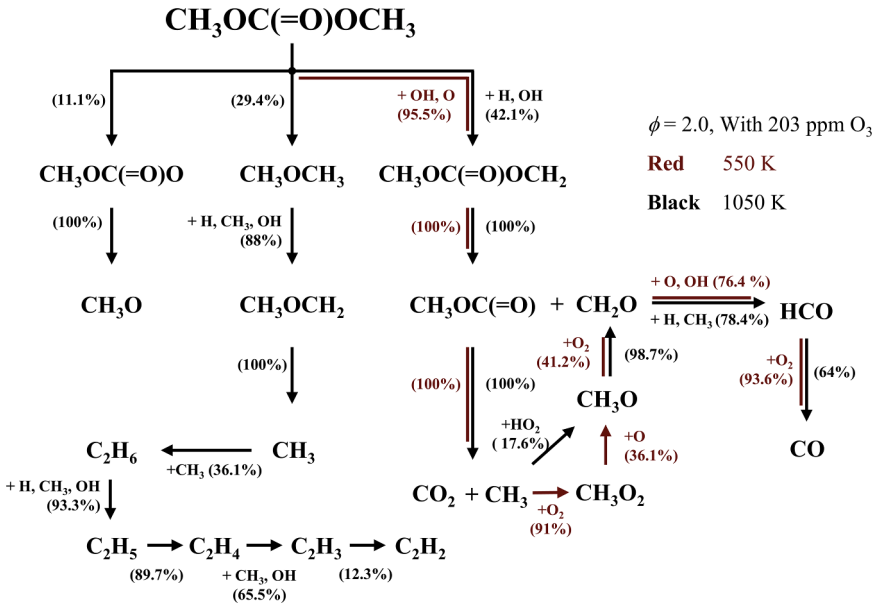

Fig. 6. The main consumption channels of DMC under low and high temperature at $\phi = 2.0$ with 203 ppm O_3 addition using Sun's model. Red and black fonts represent the percentage at 550 K and 1050 K, respectively.

reactions rates, for example from temperature increase, affect the DMC concentration negligibly. It also confirms the TIC behavior of DMC with O_3 addition. At 1050 K in Fig. 7(b), it is seen that the reaction of O_3 decomposition is not sensitive as O_3 almost disappears above 550 K in Fig. 3(c). The pyrolysis reaction of DMC is dominant for the DMC consumption.

4. Conclusions

The ozone-sensitized low- and high-temperature oxidation of DMC was carried out using an atmospheric pressure JSR from 400 to 1200 K. Kinetic analysis of the oxidation of DMC under different conditions was performed using the coupled PFR-PSR module.

The O_3 addition enhances the low-temperature reactivity of DMC significantly. Experimental results show that, without O_3 addition, the oxidation of DMC begins from 950 K with no low-temperature reactivity, while with O_3 addition, low-temperature chemistry of DMC is observed from 450 K. Two kinetic models with the addition of the O_3 sub-model were employed and predicted the experimental data reasonably well, even though slightly overpredicted DMC oxidation above 550 K under the fuel-lean condition. Furthermore, both experimental and simulation results revealed a temperature-independent coefficient (TIC) behavior of DMC with O_3 addition between 600 and 950 K. This behavior was associated with the pyrolysis of DMC radicals into CH_2O and CO_2. The low-temperature oxidation pathway involving O_2 addition and CO oxidation to CO_2 was negligible. The rapid pyrolysis of O_3 and DMC radicals, such as $CH_3OC(=O)OCH_2$ and $CH_3OC(=O)$, accounted for the observed TIC behavior in pathway and sensitivity analyses.

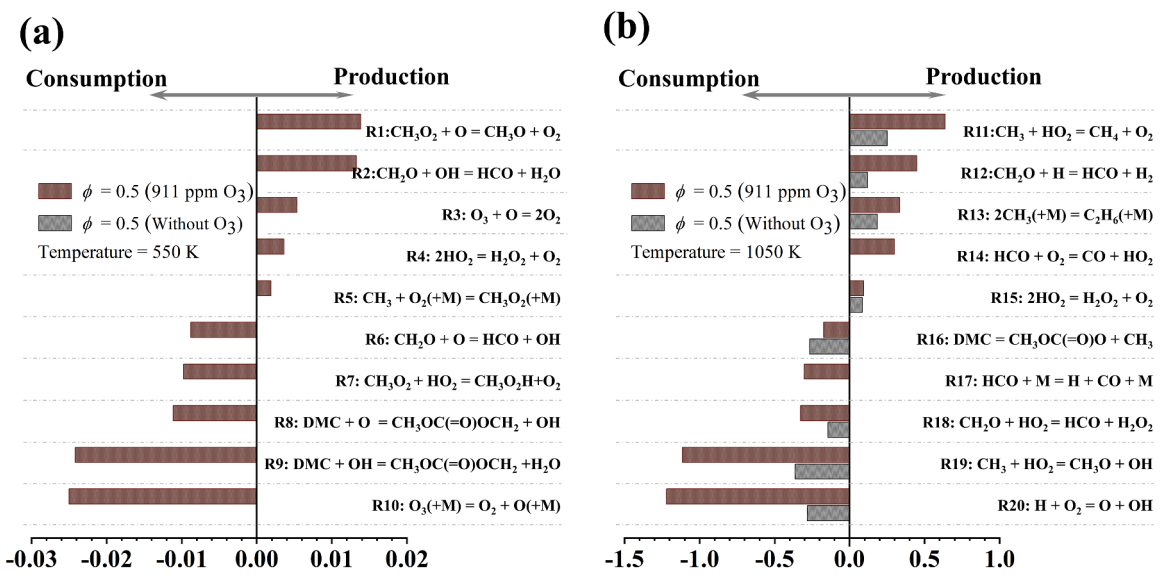

Fig. 7. Sensitivity analysis of DMC using Sun's model. (a) 550 K, $\phi = 0.5$, with and without O_3 addition; (b) 1050 K, $\phi = 0.5$, with and without O_3 addition.

In conclusion, this study used O_3 to mimic the oxidizing environment in LIBs by providing active atomic oxygen, and implied that the early degradation of LIBs could be attributed to the low-temperature oxidation of DMC with reactive oxygen species. Additionally, it provides kinetic evidence for a higher level of CO_2 and a lower level of CO in the initial stage of thermal runaway in LIBs.

Novelty and significance statement

The novelty of this research is the investigation of ozone-sensitized oxidation of dimethyl carbonate (DMC) under both low- and high-temperature conditions using an atmospheric pressure jet stirred reactor (JSR). This study uncovers a unique temperature-independent coefficient (TIC) behavior in DMC oxidation, demonstrating the enhanced reactivity of DMC at low temperature with ozone addition, and the predominant role of the pyrolysis of DMC radicals in CO_2 formation. It is significant because these findings provide new insights into the mechanisms of thermal runaway in lithium-ion batteries (LIBs), particularly in relation to gas generation and heat buildup. These findings could contribute to developing improved safety strategies for LIBs under abusive conditions, such as overcharging or thermal stress.

CRediT authorship contribution statement

Bowen Liu: Writing – review & editing, Writing – original draft, Software, Methodology, Investigation, Conceptualization. **Rui Bo:** Methodology, Investigation, Conceptualization. **Hao Zhao:** Writing – review & editing, Methodology, Supervision, Project administration.

Declaration of competing interest

The authors declare that they have no known competing financial interests or personal relationships that could have appeared to influence the work reported in this paper.

Acknowledgements

This work was supported by the National Key R&D Program of China grant (2022YFB2502100), the National Natural Science Foundation of China (No. 22361132538, No. 22350710788), the Fund of Ministry of Education (No. 8091B032244).

Supplementary materials

Supplementary material associated with this article can be found, in the online version, at doi:10.1016/j.proci.2025.105788.

References

[1] L. Lu, X. Han, J. Li, J. Hua, M. Ouyang, A review on the key issues for lithium-ion battery management in electric vehicles, J. Power Sources 226 (2013) 272–288.
[2] B. Nie, Y. Dong, L. Chang, The evolution of thermal runaway parameters of lithium-ion batteries under different abuse conditions: a review, J. Energy Storage 96 (2024) 112624.
[3] H. Wang, H. Xu, Z. Zhang, et al., Fire and explosion characteristics of vent gas from lithium-ion batteries after thermal runaway: a comparative study, ETransportation 13 (2022) 100190.
[4] Q. Wang, P. Ping, X. Zhao, et al., Thermal runaway caused fire and explosion of lithium ion battery, J. Power Sources 208 (2012) 210–224.
[5] N.E. Galushkin, N.N. Yazvinskaya, D.N. Galushkin, Mechanism of thermal runaway in lithium-ion cells, J. Electrochem. Soc. 165 (2018) A1303–A1308.
[6] T. Atherley, S. de Persis, N. Chaumeix, et al., Laminar flame speed and shock-tube multi-species laser absorption measurements of dimethyl carbonate oxidation and pyrolysis near 1 atm, Proc. Combust. Inst. 38 (2021) 977–985.
[7] K. Alexandrino, M.U. Alzueta, H.J. Curran, An experimental and modeling study of the ignition of dimethyl carbonate in shock tubes and rapid compression machine, Combust. Flame 188 (2018) 212–226.
[8] E. Hu, Y. Chen, Z. Zhang, et al., Experimental and kinetic study on ignition delay times of dimethyl carbonate at high temperature, Fuel 140 (2015) 626–632.
[9] W. Sun, B. Yang, N. Hansen, et al., An experimental and kinetic modeling study on dimethyl carbonate (DMC) pyrolysis and combustion, Combust. Flame 164 (2016) 224–238.
[10] S. Suzuki, A. Matsugi, Experimental and modeling study of fuel-rich oxidation of gasoline surrogate components/dimethyl carbonate blends in an atmospheric flow reactor, Combust, Flame 261 (2024) 113332.
[11] K. Alexandrino, Á. Millera, R. Bilbao, et al., Gas and soot formed in the dimethoxymethane pyrolysis. Soot characterization, Fuel Process. Technol. 179 (2018) 369–377.
[12] K. Alexandrino, J. Salinas, Á. Millera, et al., Sooting propensity of dimethyl carbonate, soot reactivity and characterization, Fuel 183 (2016) 64–72.
[13] M.U. Alzueta, P. Salinas, Á. Millera, et al., A study of dimethyl carbonate conversion and its impact to minimize soot and NO emissions, Proc. Combust. Inst. 36 (2017) 3985–3993.
[14] P.A. Glaude, W.J. Pitz, M.J. Thomson, Chemical kinetic modeling of dimethyl carbonate in an opposed-flow diffusion flame, Proc. Combust. Inst. 30 (2005) 1111–1118.
[15] B.L.D. Rinkel, J.P. Vivek, N. Garcia-Araez, et al., Two electrolyte decomposition pathways at nickel-rich cathode surfaces in lithium-ion batteries, Energy Environ. Sci. 15 (2022) 3416–3438.
[16] J. Wandt, A.T.S. Freiberg, A. Ogrodnik, et al., Singlet oxygen evolution from layered transition metal oxide cathode materials and its implications for lithium-ion batteries, Mater. Today 21 (2018) 825–833.
[17] R. Jung, M. Metzger, F. Maglia, et al., Oxygen release and its effect on the cycling stability of $LiNi_xMn_yCo_zO_2$(NMC) cathode materials for li-ion batteries, J. Electrochem. Soc. 164 (2017) A1361–A1377.

[18] H. Zhao, S. Liu, C. Yan, et al., Studies of ozone-sensitized low- and high-temperature oxidations of diethyl carbonate, J. Phys. Chem. A 125 (2021) 1760–1765.
[19] Y.S. Duh, Y. Sun, X. Lin, et al., Characterization on thermal runaway of commercial 18650 lithium-ion batteries used in electric vehicles: a review, J. Energy Storage 41 (2021) 102888.
[20] Y. Wang, Y. Lin, S. He, et al., Singlet oxygen: properties, generation, detection, and environmental applications, J. Hazard. Mater. 461 (2024) 132538.
[21] W. Sun, X. Gao, B. Wu, et al., The effect of ozone addition on combustion: kinetics and dynamics, Prog. Energy Combust. Sci. 73 (2019) 1–25.
[22] P. Dagaut, M. Cathonnet, J. Rouan, et al., A jet-stirred reactor for kinetic studies of homogeneous gas-phase reactions at pressures up to ten atmospheres (≈ 1 MPa), J. phys. E 19 (1986) 207.
[23] J. Orphal, J. Staehelin, J. Tamminen, et al., Absorption cross-sections of ozone in the ultraviolet and visible spectral regions: status report 2015, J. Mol. Spectrosc. 327 (2016) 105–121.
[24] CHEMKIN-PRO, Release 15112, 422, Reaction Design, Inc, San Diego, CA, 2011, p. 396.
[25] H. Zhao, X. Yang, Y. Ju, Kinetic studies of ozone assisted low temperature oxidation of dimethyl ether in a flow reactor using molecular-beam mass spectrometry, Combust. Flame 173 (2016) 187–194.
[26] Y. Fernandes, A. Bry, S. de Persis, Identification and quantification of gases emitted during abuse tests by overcharge of a commercial Li-ion battery, J. Power Sources 389 (2018) 106–119.